

---

## Thermal oxidation of Poly(dicyclopentadiene)– kinetic modeling of double bond consumption

Huang Jing <sup>1</sup>, David Adelina <sup>2</sup>, Le Gac Pierre Yves <sup>2</sup>, Lorthioir Cedric <sup>3</sup>, Coelho Cristina <sup>4</sup>,  
Richaud Emmanuel <sup>1,\*</sup>

<sup>1</sup> Laboratoire PIMM, Arts et Métiers, CNRS, Cnam, HESAM Université, 151 Boulevard de l'Hôpital, F-75013, Paris, France

<sup>2</sup> IFREMER, Service Matériaux et Structures, Centre de Brest BP70, F-29280, Plouzané, France

<sup>3</sup> Sorbonne Université, CNRS, Collège de France, Laboratoire de Chimie de la Matière Condensée de Paris, LCMCP, 4 Place Jussieu, F-75005, Paris, France

<sup>4</sup> Sorbonne Université, CNRS, Institut des Matériaux de Paris Centre, FR 2482, F-75005, Paris, France

\* Corresponding author : Emmanuel Richaud, email address : [emmanuel.richaud@ensam.eu](mailto:emmanuel.richaud@ensam.eu)

---

### Abstract :

This paper reports chemical changes that occur in polydicyclopentadiene during thermal oxidation at several temperatures and oxygen pressures. A particular attention was paid to the double bond consumption since these latter are associated with crosslinking and subsequent changes in mechanical properties. A kinetic model was derived from the experimental results. Its rate constants were assessed from the “inverse approach” based on their selective identification under specific ageing conditions (for example under oxygen excess). The resulting model satisfactorily describes both carbonyl formation and double bond consumption for a wide range of temperature and oxygen pressure for the first time. This can be exploited to predict the changes of local mechanical properties.

### Highlights

► Experimental study of PDCPD thermal oxidation in the 20-120 °C temperature range with varying oxygen partial pressures (0.02–2.0 MPa). ► Changes in stable products (carbonyls), double bonds and intermediate species (POOH). ► Kinetic modeling with selective identification of rate constants ► Link with changes in mechanical properties.

**Keywords :** Polydicyclopentadiene, Thermal oxidation, Kinetic modeling, crosslinking

## 1. Introduction

Polydicyclopentadiene (PDCPD) is obtained by metathesis of dicyclopentadiene, as illustrated in Figure 1. This polymerization mechanism (for which the Nobel Prize in Chemistry was awarded to Chauvin, Grubbs and Schrock in 2005 [1,2]) presents several interests, especially the possibility to prepare a bulk material from a low-viscosity reactive mixture in a short processing time (ca 1 min), without the requirement of external heating. The specificity of this polymerization mechanism is to keep the concentration of double bonds almost unchanged compared to the monomer.

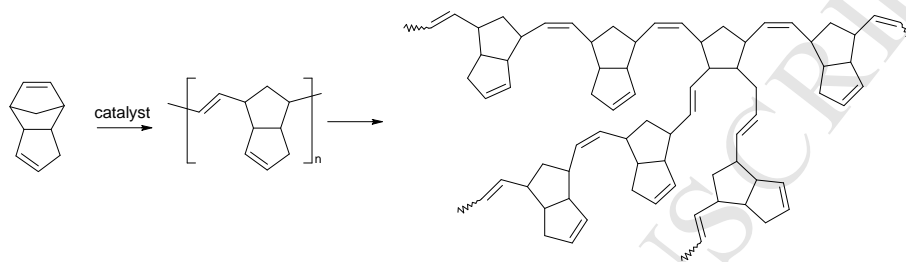


Figure 1. Polymerization of polydicyclopentadiene.

It is well established [3] that the mechanical properties of thermoset polymers depend on:

- cohesive properties (for elastic modulus) which can change during oxidation due to the appearance of new chemical groups (ketones, carboxylic acids...);
- sub-glassy mobility (not always evidenced in PDCPD) for toughness.
- crosslink density (for glass transition and yield properties) which can change with crosslinking or chain scissions.

Many authors have emphasized the effects of thermal oxidation [4] and crosslinking [5] on physical and mechanical properties through experiments (e.g. Tg, rubbery modulus, tensile properties). A recent article [6] reported that the oxidation of PDCPD induces an increase of the rubbery modulus which indicates an oxidation induced crosslinking process. Several reactions can be considered to explain this behavior since both alkyl radicals ( $P^\bullet$ ) and peroxy radicals ( $POO^\bullet$ ) are very reactive and can participate in the coupling between two radicals by a termination process or the reaction with a double bond in a similar way to elastomer oxidation [7].

A reliable lifetime prediction of PDCPD thus requires an accurate description of crosslink density during oxidation. In this contribution, our aim is to monitor the chemical modifications involved in PDCPD crosslinking during its thermal oxidation. Such information will allow a better understanding of the interplay with the variations of the mechanical behavior observed for aged polymers. For this purpose, we will complete the previously established kinetic model [8] by considering reactions involving the PDCPD double bonds and determining their rate constants. Since crosslinking and double bond consumption can originate from reactions with either P° or POO° species, our strategy relies on the comparison of the aging behavior under air and under different oxygen pressures [9,10] (which is a way to isolate the specific contribution of some rate constants) following a similar approach to the one used previously for polybutadiene [11] and polychloroprene [12]. Such an experimental approach should help achieve a better separation of the contributions from these two types of reactions. To facilitate this resolution, some approximated analytical calculations, that are intended to orientate the numerical solution, will first be carried out. The extent of agreement between both numerical simulations and analytical solutions will be considered.

## 2. Experimental

### 2.1 Material

The poly(dicyclopentadiene) samples under investigation (Telene 1810, Telene SAS) were supplied as a stabilized bulk material prepared by reaction injection molding process (RIM) at about 40°C. The catalyst used for the metathesis polymerization is a ruthenium salicylaldehyde phenylindenyldiene complex. By cutting the bulk material with a microtome (RM 2255 Leica), films having a thickness lower than 10 µm were obtained and these were then purified by refluxing in CH<sub>2</sub>Cl<sub>2</sub> (ref 270997 ≥ 99.8 %, Sigma-Aldrich) overnight. It is important to note that this thickness is low enough to avoid the Diffusion-Limited Oxidation effects [13]. Unstabilized samples were stored at -20°C before ageing.

96% cyclopentene (ref 344508 96 %, Sigma-Aldrich), cis-1,4-polybutadiene (ref 181374 Sigma-Aldrich) and polybutadiene (ref 181382 Sigma-Aldrich) were used as model (macro)molecules. The cis-1,4, trans-1,4, and vinyl-1,2 unit contents of both homopolymers of polybutadiene (from supplier data) are provided in Table 1.

Sample	Microstructure (%)		
	cis-1,4	trans-1,4	vinyl-1,2
PB1	98		2
PB2	36	55	9

Table 1. The microstructure of the polybutadiene homopolymers considered.

## 2.2 Exposure conditions

Two distinct kinds of exposure conditions are considered in this study. Samples were exposed at various temperatures (30°C, 50°C, 70°C), either in air-ventilated ovens at atmospheric pressure or in autoclaves at different oxygen pressures between 0.2 MPa and 1 MPa. Exposures at 20°C were performed in air-conditioned room of the lab.

## 2.3 Preparation and characterization

### 2.3.1. Fourier Transform InfraRed Spectroscopy

The FTIR spectra were collected on a Frontier spectrometer (PerkinElmer), as the average of 4 scans performed over a spectral range from 400 to 4000  $\text{cm}^{-1}$ , with a resolution of 4  $\text{cm}^{-1}$ . Spectra were then analyzed with Spectrum™ software.

The concentrations of carbonyls generated by oxidation were calculated using the Beer-Lambert equation with a molar absorptivity of 300  $\text{mol}^{-1} \text{cm}^{-1}$  [4] at 1710  $\text{cm}^{-1}$ . The double bond concentration methods will be detailed later.

To better assess this latter, some comparisons were made with:

- Cyclopentene: a few drops were placed on a KBr window with an optical path of 0.05 mm (ref 1921 supplied by Eurolabo) to verify the assignment of the absorption bands from the carbon-carbon double bonds and to calculate their molar absorptivities.

- Polybutadienes: cast on a KBr disk from a chloroform solution. The analyses, performed after complete solvent evaporation, aimed at verifying the assignment of the absorption bands from the carbon-carbon double bonds.

### 2.3.2. Differential Scanning Calorimetry

The hydroperoxide concentration was measured using a Q10 DSC calorimeter (TA Instrument) driven by Q Series Explorer™ software [14,15]. Temperature and enthalpy calibrations were first calibrated with an indium standard. Approximately 0.3 mg of virgin or oxidized samples were heated from 20 to 300°C, at a heating rate of 10°C min<sup>-1</sup>, in a sealed aluminium pan. This heating procedure was performed under an inert atmosphere obtained using nitrogen as a purge gas at a flow rate of 50 ml min<sup>-1</sup>. Results were processed using the TA Analysis software. The values of exotherms ascribed to hydroperoxides were converted into concentrations using  $\Delta H = 440 \text{ kJ mol}^{-1}$  [8].

### 2.3.3. SO<sub>2</sub> treatment

Degraded samples (5 mg) were placed in closed vessels and immersed in solutions of 5 mg of Na<sub>2</sub>SO<sub>3</sub> (ref 71988 Sigma Aldrich) in 10 ml HCl (ref 40253 Sigma Aldrich, 37 wt % in H<sub>2</sub>O) in which SO<sub>2</sub> was generated in situ for 24 hours at room temperature [14].

### 2.3.4. Solid-state NMR

<sup>1</sup>H solid-state NMR spectroscopy was used to determine the carbon-carbon double bond concentration. The NMR measurements were performed on a Bruker Avance III NMR spectrometer operating at a <sup>1</sup>H Larmor frequency of 700.14 MHz, equipped with an ultrafast MAS 1.3 mm double-resonance <sup>1</sup>H-X probe spinning up to 67 kHz. <sup>1</sup>H one-pulse experiments were carried out with a 90°(<sup>1</sup>H) pulse length of 2.0 μs and the recycle delay was varied between 20 s and 120 s, depending on

the  $T_1(^1\text{H})$  relaxation. The  $^1\text{H}$  chemical shift values were referenced using adamantane as an external reference (1.91 ppm with respect to TMS).

### 2.3.5. Tensile Tests

Tensile tests were performed using 60  $\mu\text{m}$  thick samples in order to obtain homogeneous oxidation through the sample thickness. Samples were cut in a dogbone shape with an initial working length of 10 mm. They were tested after several ageing durations at 80°C in air using an Instron test machine with a 50 N load cell and strain measured by Digital Image Correlation. For each condition, at least 8 samples were characterized in order to ensure reliability of results.

## 3. Results

### 3.1. Detection and quantification of hydroperoxides

The changes in chemical structures of PDCPD exposed at 50 °C under air were monitored by FTIR spectroscopy. An increase of the absorption band at ca 3400  $\text{cm}^{-1}$ , corresponding to hydrogen-bonded hydroxyl groups, is observed on Figure 2a. This broad band results from various species such as hydroperoxides, alcohols or carboxylic acids, all of which are oxidation products occurring in the thermal oxidation of other hydrocarbon polymers [14]. It is however difficult to distinguish these different species, based on the FTIR data.

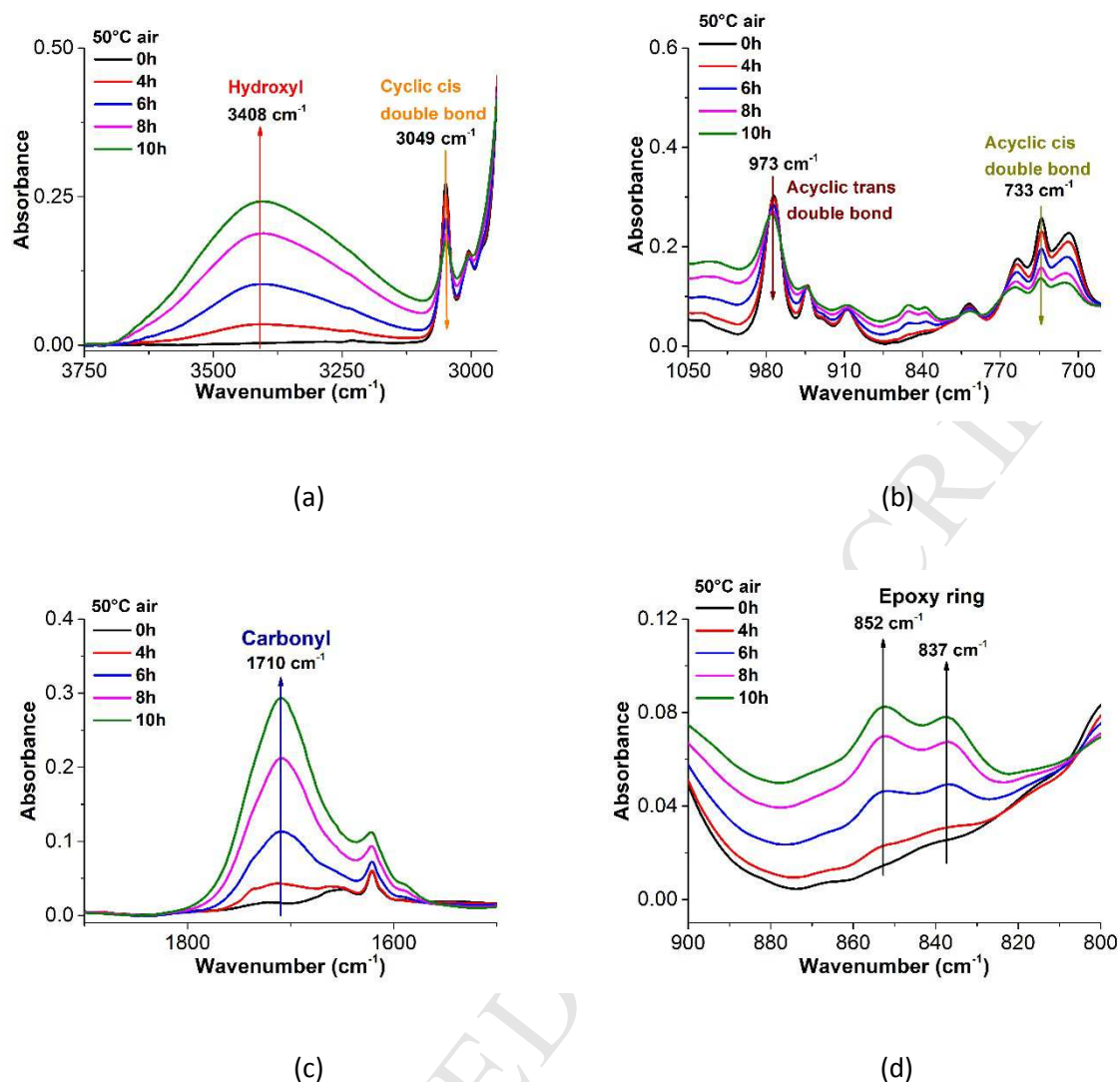
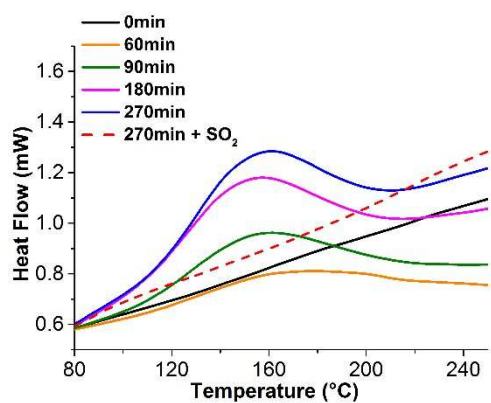
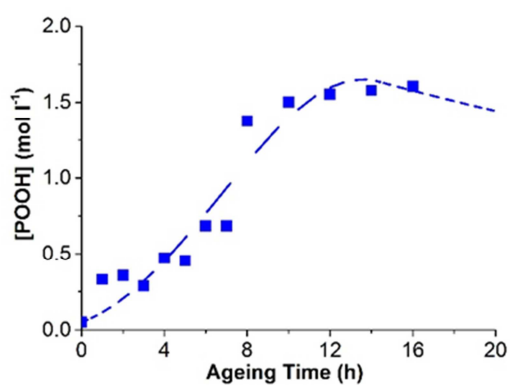


Figure 2. Changes in the FTIR spectra of PDCPD exposed at 50 °C in air.

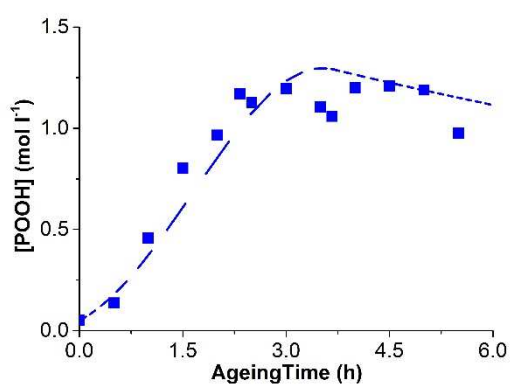
Hydroperoxides, which are the key species of the oxidation mechanism, can also be selectively detected and quantified by other chemical or thermal methods [14]. The DSC traces of PDCDP samples oxidized at 70 °C, reported in Figure 3a, show that the enthalpy change for the exotherm centered at about 150°C increases with the exposure time. Moreover, this exotherm disappears upon treatment by sulfur dioxide (Figure 3a). It is noteworthy that no residual exotherm was detected after SO<sub>2</sub> treatment for several PDCDP samples subjected to thermal oxidation at varying temperatures (50 and 70°C) and times corresponding to the maximal enthalpy release (10 h at 50°C and 4h at 70°C).



(a)



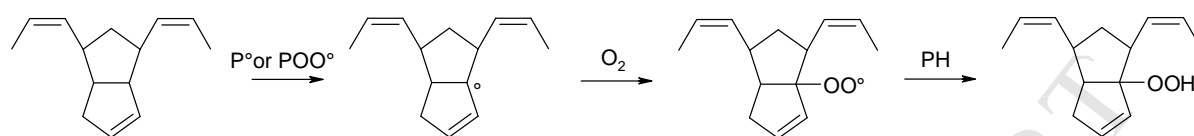
(b)



(c)

Figure 3. DSC thermograms for purified PDCPD samples before oxidation (—), and after oxidation for various exposure times at 70 °C, followed by SO<sub>2</sub> treatment (---) (a); Changes in hydroperoxide concentration with the ageing time measured by DSC (■) and simulation runs (----) at 50°C (b) and at 70°C (c).

This exotherm is hence attributed to the decomposition of hydroperoxides (POOH) depicted in Figure 4, the formation of which results from the propagation step schematized in Scheme 1.



Scheme 1. Propagation step: hydrogen abstraction.

It should be noted that several kinds of hydroperoxides can actually be formed (Figure 4). The relative probability of each kind of hydroperoxide (depending at least on bond dissociation of the C-H precursor, and hindrance) will not be discussed here.

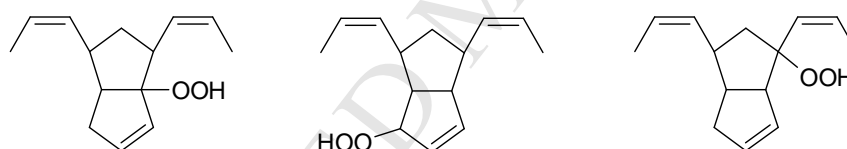


Figure 4. Possible structures of hydroperoxides formed within a thermally-oxidized PDCDP.

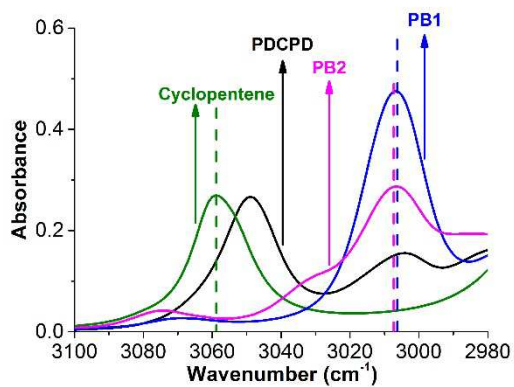
The POOH concentration was assessed from the value of the exotherm. Figure 3b shows, for 50°C and in Figure 3c for 70°C, the growth curve of hydroperoxides as a function of the aging time, which has been confirmed experimentally by other authors [16].

### 3.2 Concentration of double bonds

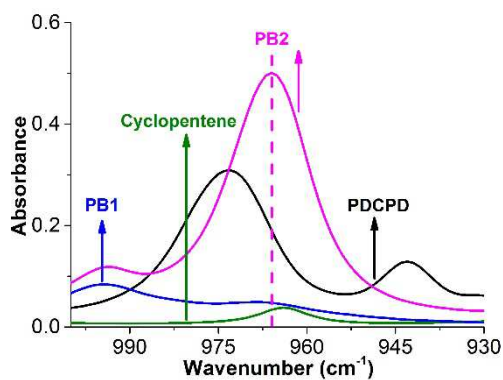
① In virgin PDCPD

Since the concentration of double bonds in the unaged PDCPD is needed in order to propose a kinetic model, FTIR experiments were first used to determine this quantity. The assignment of characteristic absorption bands for double bonds, reported in Figure 2a and 2b, has been verified using model molecules (cyclopentene and polybutadiene homopolymers, Figure 5) and was found to be in agreement with the literature. More precisely, the peak at  $3049\text{ cm}^{-1}$  (Figure 2a) is attributed to  $\omega(=C-H)$  for cyclic cis double bonds, as confirmed by the FTIR spectrum of cyclopentene (Figure 5a) [17,18]. The peak at  $973\text{ cm}^{-1}$  is related to  $\omega(=C-H)$  for acyclic trans double bonds, as also observed for a polybutadiene homopolymer with 55 % of trans-1,4 units (Figure 5b) [17,19,20].

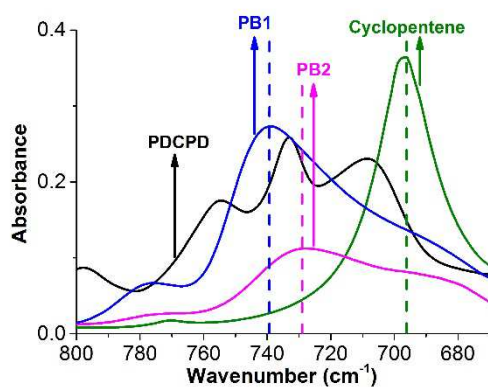
The cis =C-H wagging bands for cis dialkyl ethylenes are located in the  $720\text{--}680\text{ cm}^{-1}$  region, even though this band is less dependable for structural elucidation [20]. Two peaks may be observed on the FTIR spectrum of PDCPD near this range, at  $733$  and  $709\text{ cm}^{-1}$  (Figure 5c). Nava and al. [19] proved that polybutadienes differing by their 1,2 vinyl, 1,4 cis and 1,4 trans content always display a medium-strong band in the  $728\text{--}750\text{ cm}^{-1}$  region corresponding to cis  $\omega(=C-H)$  so that the band at  $733\text{ cm}^{-1}$  is attributed to acyclic cis double bonds [3].



(a)



(b)



(c)

Figure 5. Comparison of the FTIR spectra of purified, unaged PDCPD (in black) and model systems: cyclopentene (in green), cis-1,4-polybutadiene (in blue) and polybutadiene (36 % of cis-1,4 units, 55 % of trans-1,4 units and 9 % of vinyl-1,2 units) (in magenta).

The total double bond concentration within PDCPD is the sum of three contributions corresponding to cyclic cis -HC=CH- bonds, acyclic cis -HC=CH- bonds and acyclic trans -HC=CH- bonds:

$$[C = C] = [C = C]_{\text{cyclic cis double bond}} + [C = C]_{\text{acyclic cis double bond}} + [C = C]_{\text{acyclic trans double bond}}$$

Using values of molar absorptivity equal to  $19 \text{ l mol}^{-1} \text{ cm}^{-1}$  for cyclic cis -H=C,  $60 \text{ l mol}^{-1} \text{ cm}^{-1}$  for cis vinylene units (R-CH=CH-R') [21], and  $100 \text{ l mol}^{-1} \text{ cm}^{-1}$  for trans vinylene units (R-CH=CH-R') [22], this concentration can be expressed as:

$$[C = C] = \frac{[= C - H]_{3049}}{2} + \frac{[= C - H]_{973}}{2} + \frac{[= C - H]_{733}}{2}$$

$$= \frac{1}{2} \times \frac{1}{l} \times \left( \frac{A_{3049}}{\varepsilon_{3049}} + \frac{A_{733}}{\varepsilon_{733}} + \frac{A_{973}}{\varepsilon_{973}} \right)$$

As a result, the double bond concentration of purified, unaged PDCPD is found to be about 10-13 mol.  $\text{l}^{-1}$ . It must be acknowledged that the relative concentration of acyclic and cyclic double bonds does not match well with the expected values (their concentration should theoretically be the same) but this has a very limited consequence on the following of our work since we only will model the overall double bond decay. At room temperature, PDCPD is in the glassy state and the low extent of molecular mobility results in an inefficient motional averaging of the  $^1\text{H}$ - $^1\text{H}$  dipolar couplings and thus, in a significant broadening of the  $^1\text{H}$  NMR peaks. Such a situation renders the contribution from chemically-distinct protons difficult to resolve on the  $^1\text{H}$  NMR spectrum of bulk PDCPD. For this reason,  $^1\text{H}$  solid-state NMR experiments on PDCPD were performed at high magnetic field ( $^1\text{H}$  Larmor frequency  $\nu_0$  of 700 MHz) in order to improve the separation between the contributions from the different kinds of protons involved in unaged PDCPD. In addition, the  $^1\text{H}$  one-pulse experiments were performed under sample rotation at an ultra-fast spinning frequency ( $\nu_r = 50 \text{ kHz}$ ). The combination of both experimental conditions led to a clear separation of the peaks related to -CH= and saturated CH /  $\text{CH}_2$  protons, as shown in Figure 6, and thus enables a rather accurate quantification of the amount of double bonds. The peak at 5.6 ppm is assigned to the -CH= protons whereas the one at 2.7 ppm corresponds to the superimposition of the contributions from the saturated CH and  $\text{CH}_2$  protons. The deconvolution of the  $^1\text{H}$  NMR spectrum of unaged PDCPD (Figure 6), recorded under quantitative conditions, was performed using two components with a Voigt line shape. The ratio between the areas of these components was found to be 1.99, i.e. very close to the value expected by considering the chemical structure of PDCPD. From these solid-state NMR results, the double bond concentration for unaged PDCPD was estimated to be  $13 \text{ mol l}^{-1}$ , which is in good agreement with the value

deduced from FTIR experiments and also consistent with the theoretical value  $2 \times \rho / M_m$  ( $\rho$  is the density =  $1045 \text{ g l}^{-1}$  and  $M_m$  the molar mass of the monomer). This latter is expected to be about  $15 \text{ mol l}^{-1}$  having in mind that part of double bonds can disappear during the curing process and given the uncertainties on molar absorptivities. It is possible that the strong heat release during PDCPD polymerization induce a very high crosslinking level (consistently with the higher density value than in [23]) and the disappearance of hexahydropentalene groups. This would explain why the  $\beta$  relaxation process (associated to hexahydropentalene groups [24]) is absent in our case and why the double bond concentration is lower than  $15 \text{ mol l}^{-1}$ .

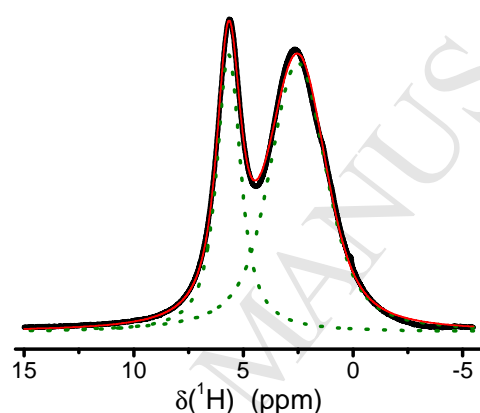
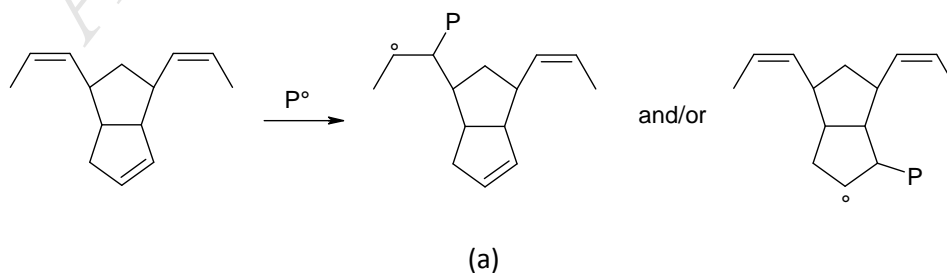
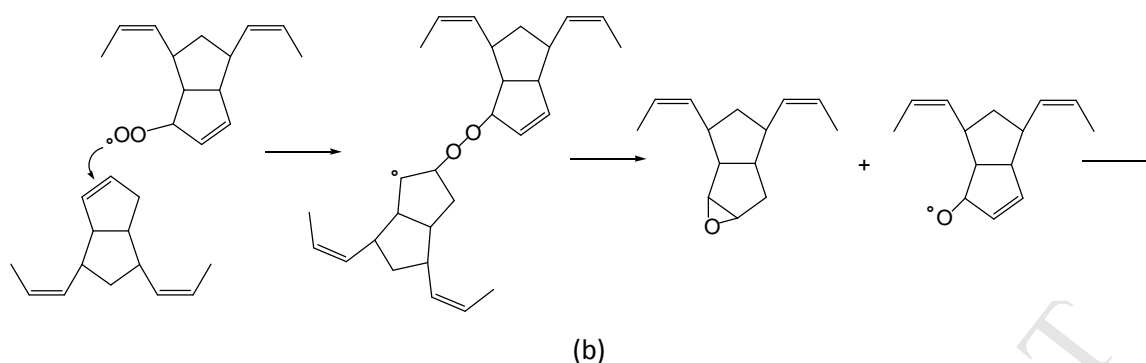


Figure 6. One-pulse  $^1\text{H}$  MAS NMR spectrum of purified, unaged PDCPD, recorded at a  $^1\text{H}$  Larmor frequency  $\nu_0$  of 700 MHz and a MAS frequency  $\nu_r$  of 50 kHz. The deconvolution of the spectrum (red solid line) using Voigt line shapes (green dotted lines) is also included.

## ② In oxidized PDCPD

The comparison of the IR spectra obtained on virgin PDCPD and PDCPD thermo-oxidized at  $50 \text{ }^\circ\text{C}$ , under air (Figure 2a, 2b) shows a decrease of the concentration of all types of double bonds, which indicates reactions between double bonds and radicals (Scheme 2).





Scheme 2. Propagation step: addition reaction of  $P^\bullet$  and  $POO^\bullet$  to double bonds. NB1: radicals can add on each side of the double bond, NB2: Intramolecular addition is not considered in the case of PDCPD due to its structural hindrance.

Addition reactions of alkyl radicals (Scheme 2a) could be a possible way of PDCPD crosslinking. This situation differs from the addition of peroxy radicals (Scheme 2b) which does not lead to crosslinking, due to the formation of epoxide products. The occurrence of the reactions depicted in Scheme 2b during the thermo-oxidation of PDCPD at 50 °C is evidenced, from an experimental point of view, by the FTIR measurements which indicate the formation of epoxides, as can be observed in Figure 2d.

Figure 7a shows the changes of the concentration of each kind of double bond as a function of the exposure time at 50°C. The corresponding consumption rates, determined as the maximal slope in Figure 7b, are compared in Table 2. Conformational effects could explain a difference in reactivity with each kind of double bond. In a first approach, we considered the values for each kind of double bond to be almost the same, so that we will assume in the following that the reactivity of each of them is ruled by the same set of rate constants (NB: this hypothesis also allows to avoid mistakes due to uncertainties on the molar absorptivities).

	$[C=C]_0$ (mol l <sup>-1</sup> )	$r_F$ (mol l <sup>-1</sup> s <sup>-1</sup> )	Relative $r_F$ (s <sup>-1</sup> )
Acyclic trans: 973 cm <sup>-1</sup>	1.91	4.24E-5	2.22E-5
Acyclic cis: 733 cm <sup>-1</sup>	0.99	3.43E-5	3.47E-5
Cyclic cis: 3050 cm <sup>-1</sup>	8.53	2.44E-4	2.86E-5

Table 2. Initial concentration consumption rate ( $v_F$ ) and relative consumption rate (relative  $r_F = r_F/[C=C]_0$ ) of the different kinds of double bonds in PDCPD.

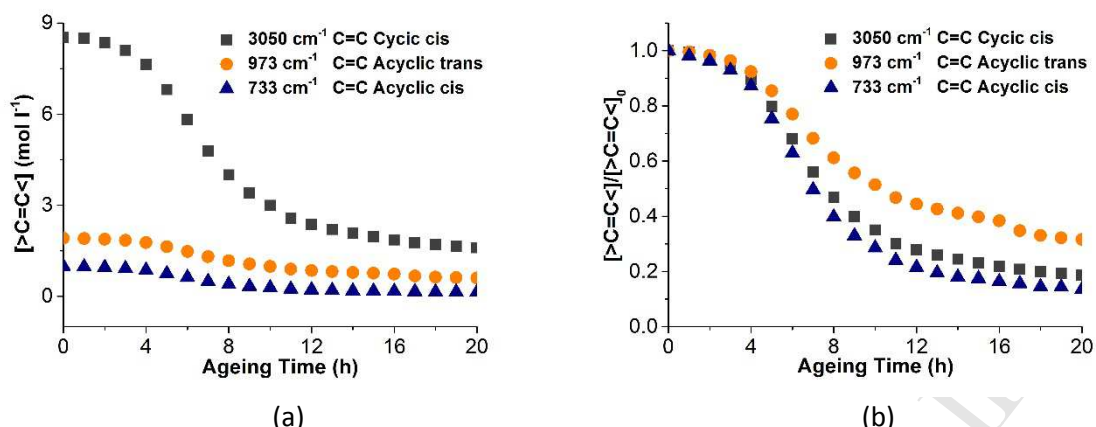
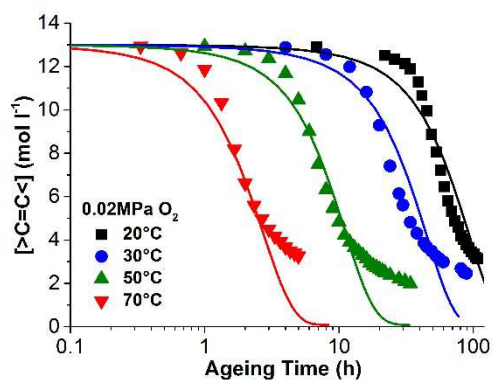
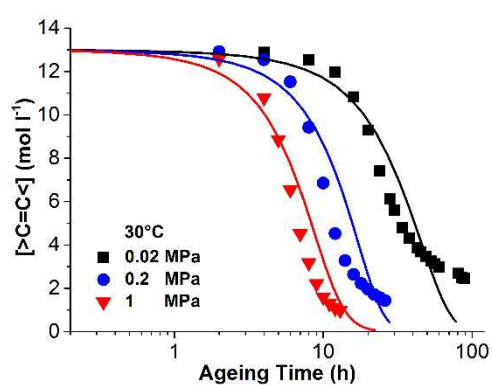


Figure 7. Variation of the absolute (a) and relative (b) concentrations of cyclic cis double bonds (band at 3050 cm<sup>-1</sup> ■), acyclic trans double bonds (band at 973 cm<sup>-1</sup> ●), and acyclic cis double bonds (band at 733 cm<sup>-1</sup> ▲) during an exposure under air at 50°C. The relative concentration values in (b) were obtained using a normalization by the corresponding concentrations of the unaged PDCPD.

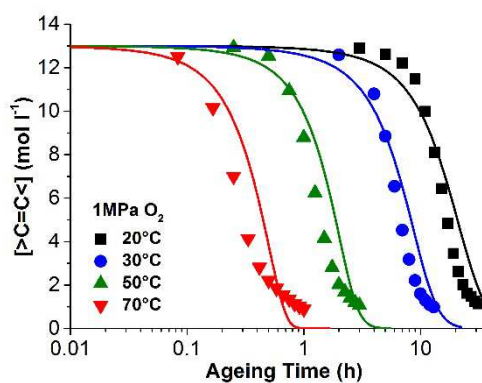
The same experiments in air were performed at other ageing temperatures (20 °C, 30 °C and 70 °C), decreases in double bonds within the aged PDCPD are reported in Figure 8a. The results obtained at a given temperature (30 °C), under different oxygen pressures, are shown in Figure 8b while Figure 8c depicts the variation of the double bond concentration with the exposure time, when the ageing is performed under 1 MPa oxygen pressure, at different temperatures. All these data indicate that the double bond consumption rate increases with temperature and oxygen pressure. Besides, the double bond consumption rates are almost the same for ageing under 0.2 MPa and 1 MPa. This feature leads us to consider oxidation under 1 MPa as “representative” of the “oxygen excess conditions” in which P° is almost instantaneously converted into POO° so that analytical assessment of some rate constants is justified (see “Discussion”).



(a)



(b)



(c)

Figure 8. Double bond consumption under various ageing conditions: in air at different temperatures (a) Double bonds consumption at 30°C under different oxygen pressures (b); Double bonds consumption under 1 MPa oxygen pressure at different temperatures (c). The solid lines correspond to the predictions by the kinetic model.

Figure 9 shows  $^1\text{H}$  NMR spectrum of PDCPD after various aging time values (4 h, 7 h and 25 h) at  $50^\circ\text{C}$  under air. After 4 h, the  $^1\text{H}$  NMR spectrum remains qualitatively similar to the one of the unaged PDCPD (Figure 9). The main difference stands in the presence of a peak of weak amplitude at 2.1 ppm. This contribution, which becomes again more significant after 7 h at  $50^\circ\text{C}$ , may be assigned to protons from  $\text{CH}$ ,  $\text{CH}_2$  or  $\text{CH}_3$  covalently linked to  $\text{C}=\text{O}$  groups. This result is in agreement with the reactions proposed in Scheme 3 and 4, as well as with the carbonyl build-up derived from FTIR measurements (Figures 10 and 11): as the  $\text{CH}_n\text{-C}=\text{O}$  protons detected by solid-state NMR, the fraction of carbonyl groups is rather low, but detectable, after 4 h at  $50^\circ\text{C}$ , that is to say just above the induction period, while after 7 h, the concentration of these species ( $\text{CH}_n\text{-C}=\text{O}$  (NMR) and  $\text{C}=\text{O}$  (FTIR)) becomes significant. Interestingly, after 7 h, another change induced by thermal oxidation may be observed on the  $^1\text{H}$  NMR spectrum. An additional contribution between the two peaks of unaged PDCPD (2.7 ppm and 5.6 ppm) can also be observed after 7 h, as a shoulder around 4.0 ppm, in the high-frequency side of the peak at 2.7 ppm. After an exposure for 25 h at  $50^\circ\text{C}$ , the amplitude of this contribution gets higher and is now detected as a well-resolved peak at 4.5 ppm, corresponding to the proton(s) from  $\text{O-CH}$  or  $\text{O-CH}_2$  groups. At this stage, it is worth noting that this peak does not result from the protons of the epoxy rings formed during the thermo-oxidation at  $50^\circ\text{C}$  (Figure 2d). These latter should indeed give rise to peaks overlapping the broad line at 2.7 ppm.

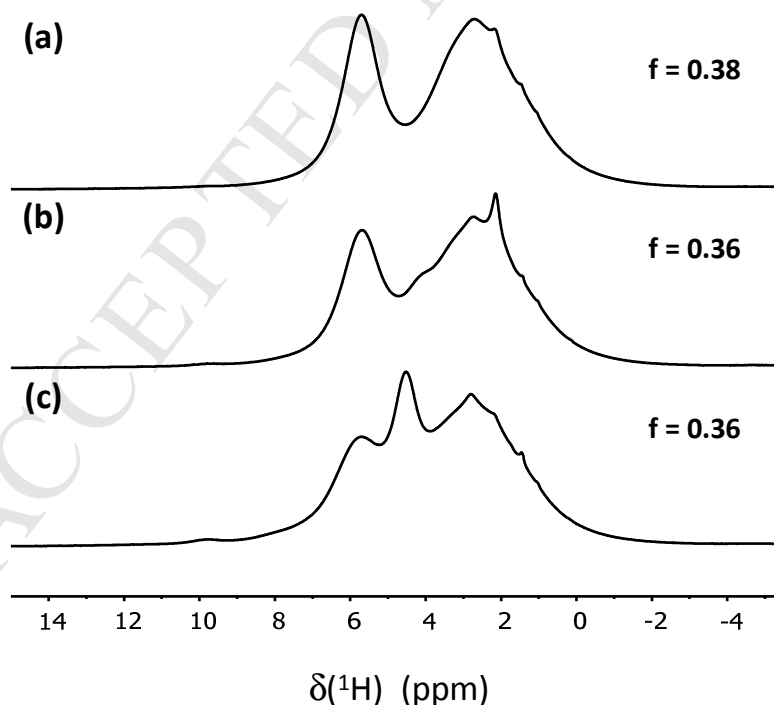


Figure 9. Changes of the one-pulse  $^1\text{H}$  MAS NMR spectrum of PDCPD thermo-oxidized at  $50^\circ\text{C}$  under air, as a function of the exposure time: (a) 4 h, (b) 7 h and (c) 25 h. The experiments were carried out at a  $^1\text{H}$  Larmor frequency  $\nu_0$  of 700 MHz and a MAS frequency  $\nu_r$  of 50 kHz. The fraction  $f$  of protons from the double bonds within aged PDCPD is also included and should be compared to  $f = 0.43$ , obtained for unaged PDCPD.

Let us now consider the variation of the double bond concentration with the aging time at 50°C. As can be seen in Figure 9, the relative amplitude of the peak at 5.6 ppm with respect to the one at 2.7 ppm decreases during aging while it also displays a significant broadening. Due to the chemical modification of the PDCPD matrix, a distribution of the local region surrounding the =CH- protons, inducing a distribution of the  $^1\text{H}$  chemical shift value, occurs. The area under the peak at 5.6 ppm should thus be considered, in order to investigate the decrease in double bond concentration with the exposure time at 50°C. The deconvolution performed in the case of the unaged PDCPD was not used because above 7 h of thermal aging, at least four contributions, with a significant overlap for some of them, are involved in the  $^1\text{H}$  NMR spectrum. The interplay between the different fitting parameters would then lead to a significant inaccuracy on the fraction  $f$  of protons involved in double bonds within aged PDCPD. To circumvent this difficulty,  $f$  was determined using half of the peak area  $A_{\text{CH=}}$ , integrating from the high frequency side down to the peak maximum frequency.  $f$  may indeed be estimated by calculating  $2 \times A_{\text{CH=}} / A_{\text{total}}$ ,  $A_{\text{total}}$  denoting the total area under the  $^1\text{H}$  NMR spectrum.

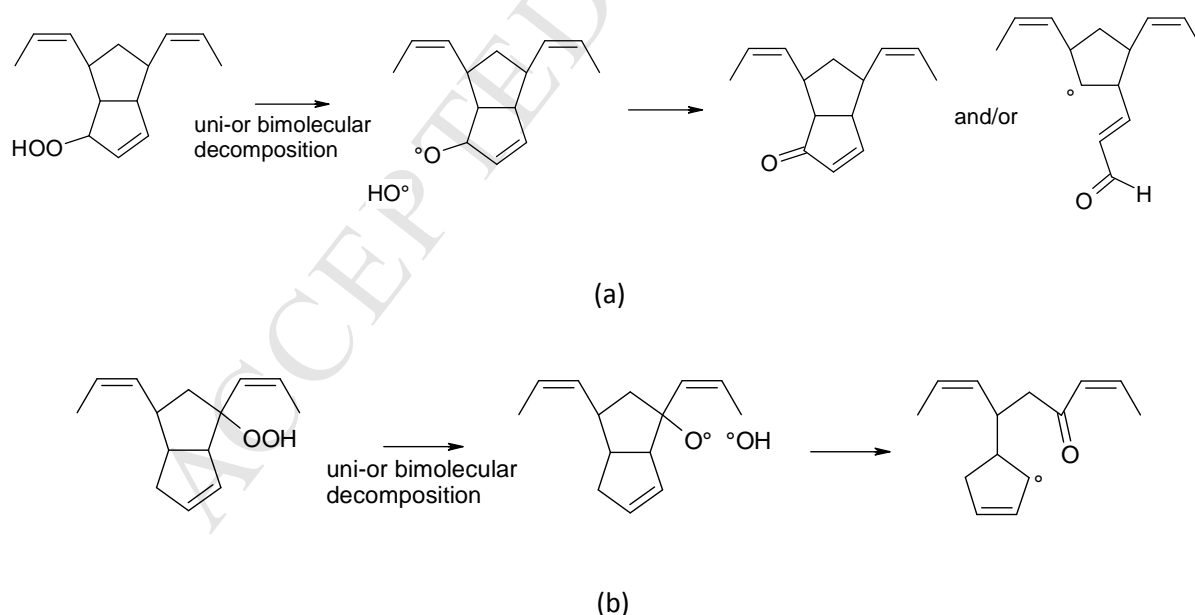
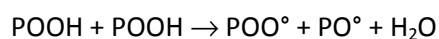
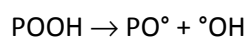
It is interesting to note that the NMR and FTIR methods give almost the same trend for samples aged for 0, 4 and 7 h. At very high oxidation levels (i.e. 25 h and more), which is not the aim of this paper, a discrepancy can be observed between NMR and FTIR. Even if it is not the subject of this study it could be possible that conjugated structures are formed and display shifted absorptions for vinyl C-H. In other words, NMR detects the total amount of residual double bonds whereas FTIR detects the unreacted ones (which is the “fuel” of the oxidation process). We however acknowledge that this argument cannot be verified in the present paper so that the mechanism of degradation at high conversion degree remains an open issue. Our approach, which considers mainly low degradation levels, is supported by the fact that mechanical behavior of PDCPD is largely affected by low levels of oxidation (Figure 12).

Lastly, one should also note that a peak at 9.7 ppm characterized by a weak, but increasing amplitude is observed on the  $^1\text{H}$  NMR spectra of the aged PDCPD (see Appendix 1). These protons may be related to carboxylic acid protons or aldehydic protons, this latter assignment being in agreement with the reactions proposed in Scheme 3.

## 3.3 Formation of carbonyls

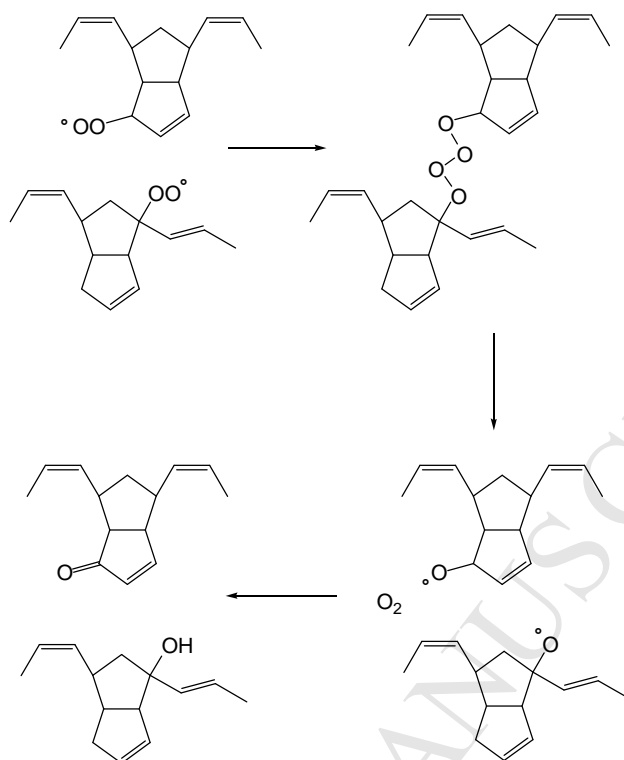
The FTIR measurements reported in Figure 2c also show the formation of a band at ca 1710  $\text{cm}^{-1}$  corresponding to carbonyl functions. As can be seen in Figure 10a, the shapes of the carbonyl band are similar under different oxidation conditions (temperature, oxygen pressure) which means that the corresponding oxidation products of PDCPD involve the same kind of carbonyl groups. They can originate from alkoxy radicals formed during:

① the initiation step during which unimolecular and bimolecular hydroperoxide decomposition can occur (Scheme 3):



Scheme 3. Initiation step: hydroperoxide decomposition.

② the termination step by disproportionation by a Russell mechanism [25,26] (Scheme 4)



Scheme 4. Termination step: Russell disproportionation of PO•.

③ the decomposition of POOP• (Scheme 2) that rearrange into PO•

The concentration in carbonyl increases with ageing time accompanied a period of induction (Figure 10b). Meanwhile, the double bond concentration decreases as a function of ageing time with a period of induction. The kinetics of carbonyl build up under several conditions are shown in Figures 11a-11c.

For all conditions considered here, carbonyl formation over ageing time follows the same behavior. First an induction period is observed where carbonyl concentration remains very low, and then a classic self-acceleration form occurs. It appears, as expected, that an increase in temperature leads to a decrease of the induction period and an increase in oxidation rate. The oxidation process can also be accelerated by increasing oxygen pressure between 0.02 MPa and 0.5 MPa (Figure 11b). Above 0.5 MPa, the oxidation process is not affected by oxygen pressure anymore showing that 0.5 MPa can be considered as the critical pressure. This behavior is observed for all ageing temperatures (Figure 11c).

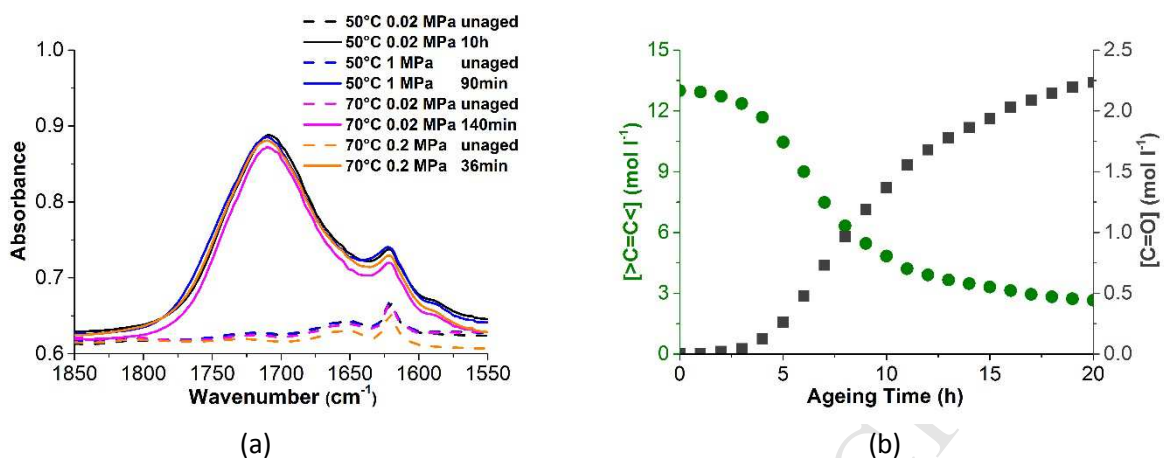
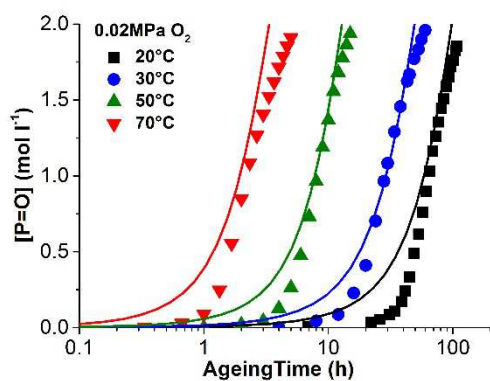
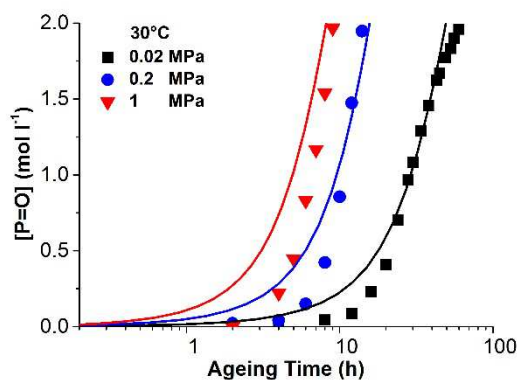


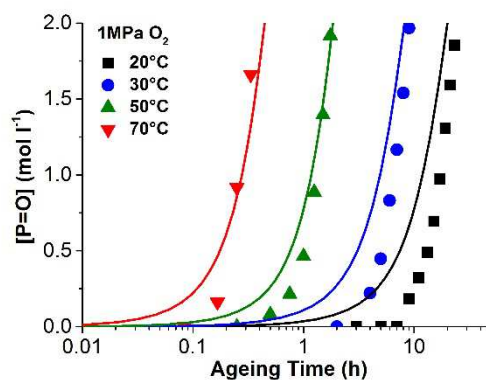
Figure 10. Infrared absorption bands of the carbonyl groups resulting from the ageing of PDCPD under various conditions (temperature, oxygen pressure) (a). Changes in the concentration of carbonyls (■) and double bonds (●) during ageing at 50 °C under air (b).



(a)



(b)



(c)

Figure 11. Variation of the carbonyl concentration as a function of the exposure time, for different ageing conditions of PDCPD: in air, at different temperatures (a); at 30 °C, under different oxygen pressures (b) under 1 MPa oxygen pressure, at different temperatures (c).

The carbonyl build-up obtained under 1 MPa oxygen pressure at different temperatures ranging between 20 °C and 70 °C (Figure 11c) also display the self-accelerated shape mentioned above.

### 3.4 Formation of epoxides

FTIR spectra of thermo-oxidized PDPCD (Figure 2d) display two bands at ca 852  $\text{cm}^{-1}$  and 837  $\text{cm}^{-1}$  that correspond to the symmetric ring deformation of epoxides. Such oxidation products are also involved in the thermo-oxidative behavior of polybutadiene [7]. The intensity of these absorption bands continuously increases during aging in air at 50 °C, but remains very weak. Consistently with NMR data (Figure 9), those species will be neglected in the following.

### 3.5 Mechanical properties

Tensile behavior of 60  $\mu\text{m}$  thick films aged at 80°C are represented in Figure 12 for several concentrations of carbonyls and double bonds. It clearly appears that oxidation leads to a decrease in strain at break as well as an increase in stress at yield. Moreover the decrease in maximal strain can be related to concentration of remaining double bonds and formed carbonyls. This means that using a model able to predict chemical changes during oxidation would allow the mechanical behavior of the polymer considered here to be evaluated.

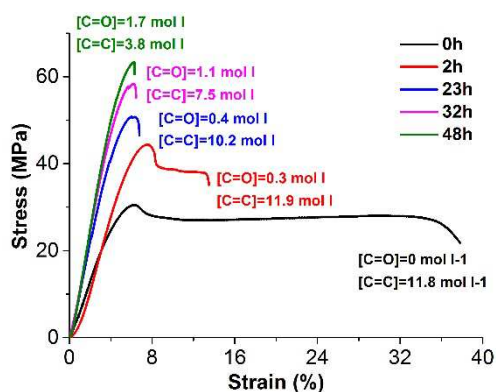


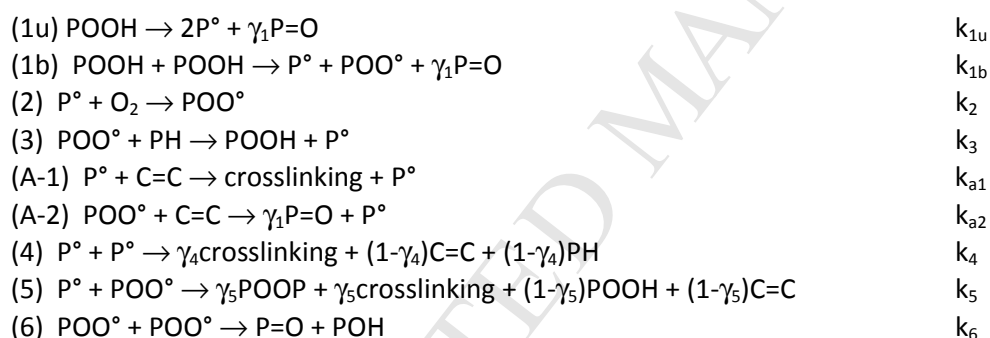
Figure 12. Tensile curves for PDPCD samples with varying exposure times at 80°C under air. NB: Concentrations were obtained by using a correction corresponding to  $\left(\frac{ACH_2}{e}\right)$  differences in samples tested for tensile tests and ageing tests monitored by FTIR.

## 4. Discussion

The aim of this section is to derive a kinetic model based on the the proposed chemical reactions and the reported chemical changes under several ageing conditions in relation to the changes in mechanical properties.

## 4.1 Proposal for a kinetic model

According to the experimental data describing chemical changes of thermo-oxidized PDCPD reported above, the following mechanistic scheme may be used for modeling the kinetic curves obtained during the ageing of PDCPD:



For summarize, it can be considered as an adaptation of the mechanistic scheme proposed by Tobolski et al [27] for the autoxidation of hydrocarbons (reactions 1u, 1b, 2, 3 and 6), together with some specific reactions for the reactivity of double bonds (reactions (a1) and (a2) [7,12,28]) and the effect of oxygen pressure (or concentration (reactions (4) and (5) [7])).

$\gamma_1$ ,  $\gamma_4$  and  $\gamma_5$  are the yields respectively for carbonyls from  $\text{PO}^\circ$  decomposition, crosslinking from  $\text{P}^\circ + \text{P}^\circ$  and  $\text{P}^\circ + \text{POO}^\circ$  coupling.

$\gamma_1$  was estimated close to 0.25 [29].  $\gamma_4$  was fixed equal to 0, and it was checked that the numerical model was found to be insensitive to the value of  $\gamma_5$  fixed equal to 0 since no POOP were detected in DSC.

$[O_2]$  can be calculated by the following equation:  $[O_2] = S_{O_2} \times P_{O_2}$ ,  $S_{O_2}$  is the solubility coefficient of oxygen in PDCPD:  $S_{O_2} = 10^{-7} \text{ mol l}^{-1} \text{ Pa}^{-1}$  [13].

In this work, the PDCPD films are thin enough (5-7  $\mu\text{m}$ ) to neglect the gradient of oxygen concentration through the thickness. The initiation step is composed of uni- and bi-molecular decompositions of POOH. It is here considered that both reactions may proceed simultaneously even if under high oxygen pressures, the oxidation is predominately bimolecular [7]. Under low oxygen pressures, the concentration of hydroperoxides is low. This feature is presently under investigation [29].

The resulting system of differential equations can be derived from the kinetic scheme (Appendix 2). It can be resolved with the following boundary values at  $t = 0$ :

$$[C=C] = [C=C]_0 \sim 13 \text{ mol l}^{-1} \text{ (adjusted from FTIR measurements).}$$

$$[PH] = [PH]_0 = 2[C=C]_0 \text{ (since each double bond is surrounded by two allylic C-H likely to react in the oxidation process).}$$

$$[P^\circ]_0 = [POO^\circ]_0 = 0.$$

$$[POOH] = [POOH]_0 = 10^{-2} \text{ mol l}^{-1}.$$

In order to solve the inverse problem, an analytical approach will be used, assuming some simplifications:

- The initiation step is considered as being predominantly bimolecular in the steady state where POOH is maximal.

- The maximum carbonyl growth rate is considered to be close to the theoretical steady-state rate, which may be calculated by assuming the substrate consumption to be negligible. Therefore, under this assumption, the steady state is considered to be reached at low conversion.

#### 4.2. Analytical solution and estimation of the termination and propagation rate constants

The steady-state regime implies that:

$$\frac{d[P^\circ]}{dt} + \frac{d[POO^\circ]}{dt} = 0 \quad (7)$$

$$\frac{d[POOH]}{dt} = 0 \quad (8)$$

Combined with equations (1), (2) and (3), these three equations become:

$$2k_{1b}[POOH]^2 = 2k_4[P^\circ]^2 + 2k_5[P^\circ][POO^\circ] + 2k_6[POO^\circ]^2 \quad (9)$$

$$2k_{1b}[POOH]^2 = k_3[POO^\circ][PH] + k_5(1 - \gamma_5)[P^\circ][POO^\circ] \quad (10)$$

In the oxygen-excess regime, the termination reactions (4), (5) and the addition reactions (A-1) can be suppressed, and the following expressions for the concentration of reactive species may be derived:

$$[POO^\circ]_\infty = \frac{k_3[PH]}{2k_6} \quad (11)$$

$$[POOH]_\infty = \frac{k_3[PH]}{2\sqrt{k_{1b} \cdot k_6}} \quad (12)$$

Therefore, the rate of carbonyl production under oxygen excess can be described by the following equation:

$$\begin{aligned} r_{ox,s} &= \frac{d[P=O]}{dt} = \gamma_1 k_{1b} [POOH]^2 + k_6 [POO^\circ]^2 + \gamma_1 k_{a2} [POO^\circ][F] \\ &= \frac{(\gamma_1 + 1)k_3^2 [PH]^2}{4k_6} + \frac{\gamma_1 k_{a2} k_3 [C=C]^2}{k_6} = \frac{(\gamma_1 + 1)k_3^2 [PH]^2}{4k_6} + \frac{\gamma_1 k_{a2} k_3 [PH]^2}{4k_6} \quad (13) \end{aligned}$$

Similarly, in the oxygen-excess regime, the consumption rate of double bonds is expressed as:

$$r_{C=C,S} = -\frac{d[C=C]}{dt} = k_{a2}[POO^\circ][C=C] = \frac{k_{a2}k_3[PH][C=C]}{2k_6} = \frac{k_{a2}k_3[C=C]^2}{k_6} \quad (14)$$

Our strategy is the following:

-  $k_2 = 10^8 \text{ l mol}^{-1} \text{ s}^{-1}$  [28] and  $k_3$  [28] are chosen from literature values.

-  $k_{1b}$  are obtained by means of the thermolysis of hydroperoxides [29].

As a result,  $k_{a2}$  and  $k_6$  may be calculated according to the following equation:

$$k_6 = \frac{(\gamma_1 + 1)k_3^2[PH]^2}{4(r_{ox,S} - \gamma_1 r_{C=C,S})} \quad (15)$$

$$k_{a2} = \frac{k_6 r_{C=C,S}}{k_3 [C=C]^2} \quad (16)$$

The values of  $k_6$  and  $k_{a2}$ , deduced from this analytical calculation, are compared with values obtained for rubbery polymers (polyisoprene [28], polychloroprene [12]) and model molecules (cyclopentene [30], indene) as shown in Figure 10. The fact that they are several orders of magnitude lower for PDCPD than for rubbery polymers and liquid compounds (Figure 13) can be discussed in terms of mobility-controlled reactions. To summarize and complete previously given explanations [6,11]:

- $POO^\circ$  reactivity is lowered because of control by segmental relaxation,
- this impacts very strongly  $POO^\circ + POO^\circ$  termination reactions.

Data from Figure 10b suggests that this effect is lower for  $POO^\circ + C=C$  reaction consistently with the fact that in such reactions,  $C=C$  are in high concentration and their reactivity is not limited by diffusion compared to  $POO^\circ + POO^\circ$  where the reactivity of the two reactants is limited by diffusion.

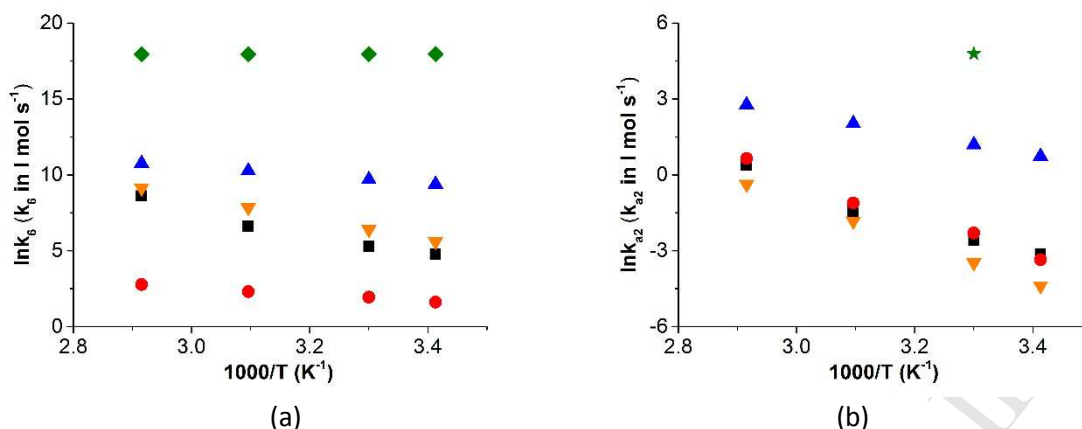


Figure 13. Arrhenius plot for  $k_6$  (a) and  $k_{a2}$  (b) for PDCPD (■, values deduced from the analytical approach; ●, values deduced from the numerical approach), polyisoprene (▲), polychloroprene-(▼), cyclopentene (◆) and indene (★) for exposure at 50°C.

#### 4.3 Numerical simulation

Following the analytical resolution of the system of equations reported in the Appendix 2, a numerical resolution has been carried out by the inverse method, without the assumptions used in Section 4.2.

In the oxygen-excess regime, only a few parameters play a role in the oxidation kinetics:  $k_{1b}$ ,  $k_2$ ,  $k_3$ ,  $k_6$  and  $k_{a2}$ . These are first estimated from the analytical approach (see previous paragraph).

Hence,  $k_{1u}$ ,  $k_4$  and  $k_5$  were estimated from the best fitting of carbonyl, double bonds and hydroperoxide concentrations in air. The value of  $k_6$  obtained analytically allows the experimental data related to the carbonyls to be modelled. However, the values of  $k_6$  and  $k_{a2}$  have been adjusted in order to account simultaneously for changes over ageing time for POOH, C=O and C=C. Figures 8c and 11c display the simulation curves for the double bond consumption and the carbonyl build-up in the oxygen-excess regime.

Table 4. Rate constants (in  $\text{l mol}^{-1} \text{s}^{-1}$  except  $k_{1u}$  in  $\text{s}^{-1}$ ) used for simulations given in Figures 3, 8 and 11. NB:  $k_{6a}$  comes from analytical calculations (Eq. 15) whereas  $k_6$  comes from numerical solution (i.e. from curve fitting).

T(°C)	$k_{1u}$ $\times 10^6$	$k_{1b}$ $\times 10^7$	$k_2$ $\times 10^{-8}$	$k_3$ $\times 10^3$	$k_4$ $\times 10^{-8}$	$k_5$ $\times 10^{-8}$	$k_6$	$k_{6,a}$	$k_{a1}$ $\times 10^{-3}$	$k_{a2}$	$k_{a2,a}$
20	1.5	1.7	1.0	3.6	5.0	1.0	5	117	6.0	0.035	0.04
30	3	3.9	1.0	9.1	5.0	1.3	7	199	7.0	0.1	0.08
50	12	18	1.0	48	5.0	1.7	10	758	9.0	0.37	0.24
70	60	70	1.0	210	5.0	2.4	16	5468	1.1	2.2	1.47
$E_a$	61	62	/	68	/	14	16	64	10	72	58
$R^2$	0.994	0.999	/	/	/	0.991	0.991	0.973	0.999	0.989	0.972

After focusing on the case of PDCPD oxidation under high oxygen pressure, the situation of oxidation under low oxygen pressure is considered. For this purpose, another addition reaction rate constant ( $k_{a1}$  corresponding to the reaction of  $P^\circ$  with  $C=C$ ) and the other termination rate constants ( $k_4$  for  $P^\circ + P^\circ$ ,  $k_5$  for  $P^\circ + POO^\circ$ ) should be determined.

Based on the results obtained under excess oxygen, the numerical simulations for PDCPD thermally-oxidized in air were more easily performed. All the values derived from the obtained by simulation in the oxygen-excess regime (i.e.  $k_{1u}$ ,  $k_{1b}$ ,  $k_2$ ,  $k_3$ ,  $k_6$ ,  $k_{a2}$  and  $\gamma_{1b}$ ) were indeed fixed. Similarly,  $k_4$  and  $k_5$  and  $k_{a1}$  can be obtained by solving the inverse problem. The numerical simulation curves describing the changes over time for carbonyls and double bonds during ageing in air are shown in Figure 7a and Figure 9a. The resulting kinetic parameters together with their activation energies are presented in Table 4. Most of the “rules” expected for kinetic parameters for radicals processes seem to be verified:  $k_4 > k_5 \gg k_6$  [31],  $E_4 \sim E_5 \sim 0 \text{ kJ mol}^{-1}$  [7,12,28],  $k_{a1} \gg k_{a2}$  [7,12,28]. The values of kinetic parameters remain to be investigated in full with the possible influence of catalyst by-products [13,29]. However, at this stage we now have a kinetic model describing the oxidation of unstabilized PDCPD in cases where oxidation is not limited by oxygen diffusion.

## 5. Conclusions

The thermal oxidation of PDCPD was studied under several temperatures and oxygen pressures. Beyond an induction period, the ageing was shown to induce a very strong decrease of the double bond concentration together with a strong increase of the carbonyl concentration. These

modifications at the chemical level are responsible for significant changes in some of the mechanical properties of thermo-oxidized PDCPD.

A kinetic model was developed on the basis of a reasonable mechanistic scheme so as to simulate and predict the chemical changes occurring in PDCPD during aging. One of the main issues associated with such kinetic models is the high number of kinetic parameters to be determined. To overcome this concern, ageing of PDCPD under oxygen excess was used to “isolate” some of the key values among the kinetic parameters. The resulting kinetic model can simulate both carbonyl build-up and double bond consumption. Since hydroperoxides are key species of the oxidation process being quantifiable without the use of adjustable parameters (such as yields from a modeling point of view, or absorptivity values from an experimental point of view), the simulation of their formation and consumption was used for a better validation of the kinetic model.

The final kinetic model appears to be suitable at least in the domain of moderate degrees of conversion and allows the extent of PDCPD degradation to be predicted with time, temperature and external oxygen pressure as input parameters. The case of stabilized PDCPD should now be addressed to get closer to practical cases [6][29].

#### ACKNOWLEDGEMENTS

Agence Nationale de la Recherche is gratefully acknowledged for having funded this study (Project VRPOM – Vieillissement des Réseaux Polymérisés par Métathèse – 2016-2019).

The French Region Ile-de-France SESAME Program is acknowledged for financial support (700 MHz spectrometer).

## APPENDIX 1

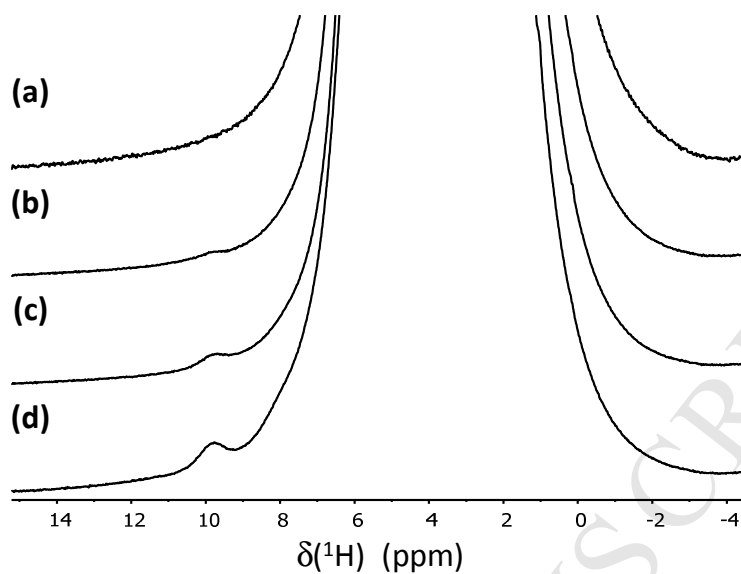


Figure S1. Zoom of the one-pulse  $^1\text{H}$  MAS NMR spectra of purified, unaged and aged PDCDP, recorded at a  $^1\text{H}$  Larmor frequency  $\nu_0$  of 700 MHz and a MAS frequency  $\nu_r$  of 50 kHz. Ageing was carried out at 50°C, under air, for: (a) 0 h, (b) 4 h, (c) 7 h and (d) 25 h.

## APPENDIX 2

$$\frac{d[POOH]}{dt} = -k_{1u}[POOH] - 2k_{1b}[POOH]^2 + k_3[POO^\circ][PH] + k_5(1 - \gamma_5)[P^\circ][POO^\circ]$$

$$\begin{aligned} \frac{d[P^\circ]}{dt} = & 2k_{1u}[POOH] + k_{1b}[POOH]^2 - k_2[P^\circ][O_2] + k_3[POO^\circ][PH] \\ & - 2k_4[P^\circ]^2 - k_5[P^\circ][POO^\circ] + k_{a2}[POO^\circ][C = C] \end{aligned}$$

$$\begin{aligned} \frac{d[POO^\circ]}{dt} = & k_{1b}[POOH]^2 + k_2[P^\circ][O_2] - k_3[POO^\circ][PH] \\ & - k_5[P^\circ][POO^\circ] - 2k_6[POO^\circ]^2 - k_{a2}[POO^\circ][C = C] \end{aligned}$$

$$\frac{d[P = O]}{dt} = \gamma_{1u}k_{1u}[POOH] + \gamma_{1b}k_{1b}[POOH]^2 + \gamma_1k_{a2}[POO^\circ][C = C] + k_6[POO^\circ]^2$$

$$\frac{d[C = C]}{dt} = -k_{a1}[P^\circ][C = C] - k_{a2}[POO^\circ][C = C] + (1 - \gamma_4)k_4[P^\circ]^2 + (1 - \gamma_5)k_5[P^\circ][POO^\circ]$$

$$\begin{aligned} \frac{d[PH]}{dt} = & -(2 - \gamma_1)k_{1u}[POOH] - (1 - \gamma_1)k_{1b}[POOH]^2 - k_3[POO^\circ][PH] \\ & - 2k_{a1}[P^\circ][C = C] - 2k_{a2}[POO^\circ][C = C] + (1 - \gamma_4)k_4[P^\circ]^2 \end{aligned}$$

## REFERENCES

- [1] Y. Chauvin, Olefin Metathesis: The Early Days (Nobel Lecture), *Angew. Chem. Int. Ed.* 45 (2006) 3740–3747. doi:10.1002/anie.200601234.
- [2] R.H. Grubbs, Olefin-Metathesis Catalysts for the Preparation of Molecules and Materials (Nobel Lecture), *Angew. Chem. Int. Ed.* 45 (2006) 3760–3765. doi:10.1002/anie.200600680.
- [3] J.-P. Pascault, H. Sautereau, J. Verdu, R.J. Williams, *Thermosetting polymers*, Marcel Dekker New York, 2002.
- [4] Y. Hu, Y. Zhang, S. Nutt, Thermal oxidation aging of polydicyclopentadiene and composites, *Polym. Compos.* 39 (2018) 1742–1751.
- [5] T.R. Long, R.M. Elder, E.D. Bain, K.A. Masser, T.W. Sirk, H.Y. Jian, D.B. Knorr, J.L. Lenhart, Influence of molecular weight between crosslinks on the mechanical properties of polymers formed via ring-opening metathesis, *Soft Matter.* 14 (2018) 3344–3360.
- [6] P.Y. Le Gac, D. Choqueuse, M. Paris, G. Recher, C. Zimmer, D. Melot, Durability of polydicyclopentadiene under high temperature, high pressure and seawater (offshore oil production conditions), *Polym. Degrad. Stab.* 98 (2013) 809–817. doi:10.1016/j.polymdegradstab.2012.12.023.
- [7] M. Coquillat, J. Verdu, X. Colin, L. Audouin, R. Nevière, Thermal oxidation of polybutadiene. Part 2: Mechanistic and kinetic schemes for additive-free non-crosslinked polybutadiene, *Polym. Degrad. Stab.* 92 (2007) 1334–1342. doi:10.1016/j.polymdegradstab.2007.03.019.
- [8] E. Richaud, P.Y. Le Gac, J. Verdu, Thermooxidative aging of polydicyclopentadiene in glassy state, *Polym. Degrad. Stab.* 102 (2014) 95–104. doi:10.1016/j.polymdegradstab.2014.01.036.
- [9] E. Richaud, F. Farcas, P. Bartoloméo, B. Fayolle, L. Audouin, J. Verdu, Effect of oxygen pressure on the oxidation kinetics of unstabilised polypropylene, *Polym. Degrad. Stab.* 91 (2006) 398–405. doi:10.1016/j.polymdegradstab.2005.04.043.
- [10] X. Colin, L. Audouin, J. Verdu, Determination of thermal oxidation rate constants by an inverse method. Application to polyethylene, *Polym. Degrad. Stab.* 86 (2004) 309–321. doi:10.1016/j.polymdegradstab.2004.04.022.
- [11] M. Coquillat, J. Verdu, X. Colin, L. Audouin, R. Nevière, Thermal oxidation of polybutadiene. Part 1: Effect of temperature, oxygen pressure and sample thickness on the thermal oxidation of hydroxyl-terminated polybutadiene, *Polym. Degrad. Stab.* 92 (2007) 1326–1333. doi:10.1016/j.polymdegradstab.2007.03.020.
- [12] P.Y. Le Gac, G. Roux, J. Verdu, P. Davies, B. Fayolle, Oxidation of unvulcanized, unstabilized polychloroprene: A kinetic study, *Polym. Degrad. Stab.* 109 (2014) 175–183. doi:10.1016/j.polymdegradstab.2014.06.019.
- [13] V. Defauchy, P.Y. Le Gac, A. Guinault, J. Verdu, G. Recher, R. Drozdak, E. Richaud, Kinetic analysis of polydicyclopentadiene oxidation, *Polym. Degrad. Stab.* 142 (2017) 169–177. doi:10.1016/j.polymdegradstab.2017.06.005.
- [14] E. Richaud, F. Farcas, B. Fayolle, L. Audouin, J. Verdu, Hydroperoxide titration by DSC in thermally oxidized polypropylene, *Polym. Test.* 25 (2006) 829–838. doi:10.1016/j.polymertesting.2006.04.010.

- [15] Y. Ouldmetidji, L. Gonon, S. Commereuc, V. Verney, A differential scanning calorimetry method to study polymer photoperoxidation, *Polym. Test.* 20 (2001) 765–768. doi:10.1016/S0142-9418(01)00024-1.
- [16] C.L. McGann, G.C. Daniels, S.L. Giles, R.B. Balow, J.L. Miranda-Zayas, J.G. Lundin, J.H. Wynne, Air Activated Self-Decontaminating Polydicyclopentadiene PolyHIPE Foams for Rapid Decontamination of Chemical Warfare Agents, *Macromol. Rapid Commun.* 39 (2018) 1800194.
- [17] M.J. Abadie, M. Dimonie, C. Couve, V. Dragutan, New catalysts for linear polydicyclopentadiene synthesis, *Eur. Polym. J.* 36 (2000) 1213–1219. doi:10.1016/S0014-3057(99)00185-8.
- [18] J. Villarreal, J. Laane, S. Bush, W. Harris, Vibrational spectra and normal coordinate analysis for cyclopentene, cyclopentene-1-d1, cyclopentene-1, 2, 3, 3-d4 and cyclopentene-d8, *Spectrochim. Acta Part Mol. Spectrosc.* 35 (1979) 331–338. doi:10.1016/0584-8539(79)80188-9.
- [19] D. Nava, T.R. de Parada, E. González, N. Boscàn, C. De La Cruz, An infrared spectroscopic comparison of cis- and trans-CH=CH and vinyl CH=CH<sub>2</sub> group frequencies of some hexenes, heptenes, and stereospecific and non-stereospecific polybutadienes, *Spectrochim. Acta. A. Mol. Biomol. Spectrosc.* 52 (1996) 1201–1210. doi:10.1016/0584-8539(96)01676-5.
- [20] D. Lin-Vien, N.B. Colthup, W.G. Fateley, J.G. Grasselli, CHAPTER 6 - Alkenes, in: *Handb. Infrared Raman Charact. Freq. Org. Mol.*, Academic Press, San Diego, 1991: pp. 73–94. doi:10.1016/B978-0-08-057116-4.50012-2.
- [21] J.G. Calvert, J.N. Pitts, *Photochemistry*, New York, 1966.
- [22] H.L. McMurry, V. Thornton, Correlation of Infrared Spectra, *Anal. Chem.* 24 (1952) 318–334. doi:10.1021/ac60062a018.
- [23] R.M. Elder, J.W. Andzelm, T.W. Sirk, A molecular simulation study of the glass transition of cross-linked poly (dicyclopentadiene) networks, *Chem. Phys. Lett.* 637 (2015) 103–109.
- [24] D.B. Knorr Jr, K.A. Masser, R.M. Elder, T.W. Sirk, M.D. Hindenlang, H.Y. Jian, A.D. Richardson, S.E. Boyd, W.A. Spurgeon, J.L. Lenhart, Overcoming the structural versus energy dissipation trade-off in highly crosslinked polymer networks: ultrahigh strain rate response in polydicyclopentadiene, *Compos. Sci. Technol.* 114 (2015) 17–25.
- [25] G.A. Russell, Deuterium-isotope Effects in the Autoxidation of Alkyl Hydrocarbons. Mechanism of the Interaction of Peroxy Radicals<sup>1</sup>, *J. Am. Chem. Soc.* 79 (1957) 3871–3877. doi:10.1021/ja01571a068.
- [26] J.A. Howard, K.U. Ingold, Self-reaction of sec-butylperoxy radicals. Confirmation of the Russell mechanism, *J. Am. Chem. Soc.* 90 (1968) 1056–1058. doi:10.1021/ja01006a037.
- [27] A.V. Tobolsky, D.J. Metz, R.B. Mesrobian, Low Temperature Autoxidation of Hydrocarbons: the Phenomenon of Maximum Rates<sup>1,2</sup>, *J. Am. Chem. Soc.* 72 (1950) 1942–1952. doi:10.1021/ja01161a023.
- [28] X. Colin, L. Audouin, J. Verdu, Kinetic modelling of the thermal oxidation of polyisoprene elastomers. Part 1: Unvulcanized unstabilized polyisoprene, *Polym. Degrad. Stab.* 92 (2007) 886–897. doi:10.1016/j.polymdegradstab.2007.01.017.

- [29] J. HUANG, Thermo oxidation of polydicyclopentadiene : determination the initiation rate constants and termination rate constants of kinetic model, (2018). <https://www.nist.gov/news-events/events/2018/03/service-life-prediction-polymeric-materials-reaching-new-heights>.
- [30] E.T. Denisov, I.B. Afanas'ev, Oxidation and Antioxidants in Organic Chemistry and Biology, Taylor & Francis, 2005.
- [31] K.T. Gillen, J. Wise, R.L. Clough, General solution for the basic autoxidation scheme, Polym. Degrad. Stab. 47 (1995) 149–161. doi:10.1016/0141-3910(94)00105-H.

ACCEPTED MANUSCRIPT

- Experimental study of PDCPD thermal oxidation in the 20-120°C temperature range with varying oxygen partial pressures (0.02 to 2.0 MPa)
- Changes in stable products (carbonyls), double bonds and intermediate species (POOH)
- Kinetic modeling with selective identification of rate constants
- Link with changes in mechanical properties

ACCEPTED MANUSCRIPT